Stability of surface contacts for humanoid robots: Closed-form formulae of the Contact Wrench Cone for rectangular support areas

Stéphane Caron, Quang-Cuong Pham, Yoshihiko Nakamura

Stability of Surface Contacts for Humanoid Robots: Closed-Form Formulae of the Contact Wrench Cone for Rectangular Support Areas

Stéphane Caron[1], Quang-Cuong Pham[2], Yoshihiko Nakamura[1]

***Abstract*— Humanoids locomote by making and breaking contacts with their environment. Thus, a crucial question for them is to anticipate whether a contact will hold or break under effort. For rigid surface contacts, existing methods usually consider several point-contact forces, which has some drawbacks due to the underlying redundancy. We derive a criterion, the Contact Wrench Cone (CWC), which is equivalent to any number of applied forces on the contact surface, and for which we provide a closed-form formula.**

It turns out that the CWC can be decomposed into three conditions: (i) Coulomb friction on the resultant force, (ii) CoP inside the support area, and (iii) upper and lower bounds on the yaw torque. While the first two are well-known, the third one is novel. It can, for instance, be used to prevent the undesired foot yaws observed in biped locomotion. We show that our formula yields simpler and faster computations than existing approaches for humanoid motions in single support, and assess its validity in the OpenHRP simulator.

I. Introduction

From a mechanical point of view, establishing contact with the environment amounts to constraining a certain number of Degrees Of Freedom (DOF) of an end-effector link. For instance, a sliding planar contact imposes three *equality* constraints (two on the orientation of the link and one for the link-to-surface distance) while a fixed contact constraints all six DOFs of the end-effector link. A stability criterion can be seen as a set of *inequality* constraints describing the conditions under which these equalities are preserved.

The Zero-Moment Point (ZMP) [1] criterion, namely that this point lies in the convex hull of ground contact points, may be the best-known example of stability criterion. It is known [2] to be necessary but *not sufficient* for contact stability, as it is accounts for neither sliding in the horizontal plane nor rotation around the vertical axis (yaw). Yet, humanoid robots are often subject to significant yaw moments during single support phases, resulting in undesired foot rotations. Attesting the importance of this problem, recent works have been using upper-body motions to compensate for these yaws while continuing to use ZMP [3], [4].

A necessary and sufficient condition for the stability of the six contact DOFs can be obtained by considering *individual contact forces* distributed on the contact surface, as can be found *e.g.*, in bipedal balance control [5] or motion planning [6], [7]. This approach is however hampered by *redundancy*: the vector of contact forces has many more components (three times the number of contact points) than the DOF of the contact constraint (six). This redundancy impedes the inversion of the equations of motion, notably the use of state-of-the-art Inverse Dynamics based on QR-decomposition [8] (which do not apply to redundant force variables)[1]. In Time-Optimal Path Parameterization (TOPP), redundancy prompted the use of further contact approximations [9] or expensive polytope projection algorithms [7]. In the present paper, we argue that such workarounds can be avoided by using a suitable contact representation (for instance, both [9] and [7] boil down to a single matrix inversion for a biped in single-support, as we will see in Section V).

The key insight here is: distributed contact forces lie in their respective friction cones if and only if the *contact wrench* belongs to a certain *wrench cone* [10], which we calculate. The contact wrench naturally solves the redundancy issue, as its dimension is minimal (six). In the context of multi-contact planning, it was advocated as a generalization of ZMP in [2] and applied to walking on rough terrains [11], [12]. However, these works made the same "sufficient friction" assumption as ZMP, meaning that the resulting criterion does not account for sliding and yaw rotations. Besides, the contact wrench was computed from individual contact forces, which we argue yields unnecessarily involved calculations: the wrench cone can be computed explicitly from the sole geometry of the end-effectors in contact.

In the present communication, we derive the closed-form formulae of the wrench cone in the case of rectangular support areas, which is of practical importance since most humanoid robot feet can be adequately approximated by rectangles. This result simplifies dynamics computations, as we will see for humanoid motions. It also provides an analytical description of *"yaw friction"*, from which we derive a control law to prevent undesirable yaw rotations.

The rest of the paper is organized as follows. In Section II, we recall the definitions related to contact stability. In Section III, we discuss the physics of surface contact and give a theoretical justification to the model where individual contact forces are applied at the vertices of the contact polygon. Then, in Section IV, we derive a closed-form expression of the wrench cone in the case of rectangular contact areas.

[1]Department of Mechano-Informatics, The University of Tokyo, Japan, caron@ynl.t.u-tokyo.ac.jp

[2]School of Mechanical and Aerospace Engineering, Nanyang Technological University, Singapore

[1] When this is not the case, the authors advocate the use of Singular Value Decomposition to compute new independent variables; however, they do not mention how to compute the inequality constraints applying to these new variables.

We apply the resulting solution in a humanoid experiment in Section V before concluding in Section VI.

II. Background

A. Contact Forces and Contact Wrench

Consider a robot with n degrees of freedom making N point contacts with the environment, at points $C_1, \dots, C_N$ in the laboratory frame. The equations of motion of the robot are:

$$\mathbf{M}(\boldsymbol{q})\ddot{\boldsymbol{q}} + \boldsymbol{h}(\boldsymbol{q}, \dot{\boldsymbol{q}}) = \mathbf{S}^\top \boldsymbol{\tau}_a + \sum_{i=1}^{N} \mathbf{J}(C_i)^\top \boldsymbol{f}_i, \qquad (1)$$

where $\boldsymbol{q}, \dot{\boldsymbol{q}}, \ddot{\boldsymbol{q}}$ are the n-dimensional vectors of DOF values, velocities and accelerations, $\mathbf{M}$ is the $n \times n$ joint-inertia matrix, $\boldsymbol{h}(\boldsymbol{q}, \dot{\boldsymbol{q}})$ the n-dimensional vector of gravity and Coriolis forces. In case the robot has n_a actuated joints, $\boldsymbol{\tau}_a$ is the n_a-dimensional vector of torques at the actuated joints and $\mathbf{S}$ is the $n_a \times n$ joint selection matrix. Finally, for each $i \in [1, N]$, $\boldsymbol{f}_i$ is a 3-dimensional vector of contact force (in the laboratory frame) and $\mathbf{J}(C_i)$ is the $3 \times n$ *translation* Jacobian calculated at point C_i.

We assume that both the environment and the contacting link are rigid bodies. Thus, interactions between them can be represented by a single *contact wrench* $\boldsymbol{w} = (\boldsymbol{f}, \boldsymbol{\tau})$, which one can compute from contact forces as:

$$\boldsymbol{f} \stackrel{\text{def}}{=} \sum_i \boldsymbol{f}_i, \qquad (2)$$

$$\boldsymbol{\tau} \stackrel{\text{def}}{=} \sum_i \overrightarrow{OC_i} \times \boldsymbol{f}_i, \qquad (3)$$

where O is the origin of the link frame. The contact jacobian $\mathbf{J}_{\text{wr}}$ is the $6 \times n$ matrix obtained by stacking vertically $\mathbf{J}(O)$, the translation Jacobian computed at O, and $\mathbf{J}_{\text{rot}}$, the *rotation* Jacobian of the link, both taken with respect to the absolute frame. With these definitions,

$$\mathbf{J}_{\text{wr}}^\top \boldsymbol{w} = \sum_{i=1}^{N} \mathbf{J}(C_i)^\top \boldsymbol{f}_i. \qquad (4)$$

(See Appendix A for calculations.) Thus, the equations of motion can be rewritten as:

$$\mathbf{M}(\boldsymbol{q})\ddot{\boldsymbol{q}} + \boldsymbol{h}(\boldsymbol{q}, \dot{\boldsymbol{q}}) = \mathbf{S}^\top \boldsymbol{\tau}_a + \mathbf{J}_{\text{wr}}^\top \boldsymbol{w}. \qquad (5)$$

B. Contact Stability

Assume now that the robot is in a given state $(\boldsymbol{q}, \dot{\boldsymbol{q}})$. Then, accelerations $\ddot{\boldsymbol{q}}$ and generalized forces (actuated torques or contact forces) are bound by a *complementarity* condition [13]. For the sake of explanation, let us describe first the case of a single translation coordinate x, as depicted in Figure 1. Under Coulomb's friction model, either of the following situations occurs :

- **Fixed contact:** $\ddot{x} = 0$ and the contact force obeys $|f_c^t| \leq \mu f_c^n$, where f_c^t and f_c^n are the horizontal and vertical components of $\boldsymbol{f}_c$ and μ is the static friction coefficient;

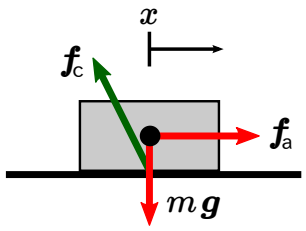

Fig. 1. Simple case of a body on a horizontal surface, with one DOF, under the action of three forces: its weight ($m\boldsymbol{g}$), the resultant contact force ($\boldsymbol{f}_c$) and its inertial force ($\boldsymbol{f}_a = [m\ddot{x}\ 0\ 0]$).

- **Sliding contact:** $\ddot{x} > 0$ and the contact force obeys $f_c^t = -\mu_k f_c^n$, where μ_k is the kinetic friction coefficient.

The acceleration $\ddot{x}$ and contact force $\boldsymbol{f}_c$ are in a *complementary* relationship: when one is equality-constrained, the other is inequality-constrained.

Similarly, when a six-DOF end-effector is in contact, its translational and rotational accelerations are in a complementary relationship with some generalized contact forces $\boldsymbol{\gamma}$ (here, $\boldsymbol{\gamma} = \boldsymbol{w}$ or $\boldsymbol{\gamma} = (\boldsymbol{f}_1, \dots, \boldsymbol{f}_N)$). The *contact mode* describes, for each variable in a complementary relationship, which of the acceleration or force variables is equality- or inequality-constrained. In the present work, we are interested in the *fixed contact mode* where the position and orientation of the end-effector are equality-constrained to a reference value, all force variables being therefore inequality-constrained.

Definition 1 (Weak Contact Stability): A contact is weakly stable when there exists a solution $(\ddot{\boldsymbol{q}}, \boldsymbol{\tau}_a, \boldsymbol{\gamma})$ of the equations of motion satisfying the fixed contact mode for all contacting links. That is to say,

- for each contact (i), the relative velocity and acceleration at contact are zero: $\mathbf{J}_{\text{wr}}^{(i)}\dot{\boldsymbol{q}} = 0$ and $\mathbf{J}_{\text{wr}}^{(i)}\ddot{\boldsymbol{q}} = -\dot{\mathbf{J}}_{\text{wr}}^{(i)}\dot{\boldsymbol{q}}$,
- actuated torques $\boldsymbol{\tau}_a$ are within torque limits,
- complementary forces $\boldsymbol{\gamma}$ satisfy their inequality constraints (friction cones or wrench cone).

This formulation has been widely used in the literature. In approaches based on inverse dynamics, the first condition is first enforced kinematically, then torques and complementary forces are solved [7], [8]. The "weakness" in the definition above refers to the notions of strong and weak stability, as stated by [13]. Strong stability happens when *all* solutions to the equations of motion satisfy the fixed contact mode.

Note that choosing between contact forces and the contact wrench changes the equations of motion (Equations (1) and (5)) but the underlying contact stability is the same by Equation (4). In the rest of the paper, we will always refer to contact stability in the weak sense.

III. Surface Contact

Suppose we take contact forces $\boldsymbol{f}_1, \dots, \boldsymbol{f}_N$ as complementary variables to the position and orientation of the contacting link. Let f_i^n and $\boldsymbol{f}_i^t$ denote the normal and the tangential components of the contact force $\boldsymbol{f}_i$. Coulomb friction provides the complementary inequalities:

- **Unilaterality:** $f_i^n > 0,$ (6)
- **Non-slippage:** $\|\boldsymbol{f}_i^t\| \leq \mu f_i^n,$ (7)

with μ is the static coefficient of friction.

However, when the contact is mediated through a surface and not through a set of points, the reality of contact is continuous. To account for this continuity, we model the action of the environment at the surface $\mathcal{S}$ by two quantities: a scalar field $p(x, y)$ corresponding to normal *pressure*, and a two-dimensional vector field $\boldsymbol{\sigma}(x, y)$ for tangential mechanical *stress*. Figure 2-(A) illustrates these two fields for a rectangular contact area. For convenience, we also will denote by $\boldsymbol{\nu} \stackrel{\text{def}}{=} \boldsymbol{\sigma}(x, y) + p(x, y)\boldsymbol{n}$, where $\boldsymbol{n}$ is the unit vector normal to the contact surface (pointing upward). The equations of motion become

$$\mathbf{M}\ddot{\boldsymbol{q}} + \boldsymbol{h} = \mathbf{S}^\top \boldsymbol{\tau}_a + \int_{\mathcal{S}} \mathbf{J}(C_{xy})^\top \boldsymbol{\nu}(x, y)\mathrm{d}x\mathrm{d}y \tag{8}$$

where $\mathbf{J}(C_{xy})$ is the $3 \times n$ translation Jacobian calculated at the point of coordinate C_{xy} on the surface. By analogy with its discrete counterpart (2)-(3), the wrench resulting from $\boldsymbol{\nu}(x, y)$ is

$$\boldsymbol{f} \stackrel{\text{def}}{=} \int_{\mathcal{S}} \boldsymbol{\nu}(x, y)\mathrm{d}x\mathrm{d}y, \tag{9}$$

$$\boldsymbol{\tau} \stackrel{\text{def}}{=} \int_{\mathcal{S}} \overrightarrow{OC_{xy}} \times \boldsymbol{\nu}(x, y)\mathrm{d}x\mathrm{d}y, \tag{10}$$

where O is the origin of the link frame. Note how the resulting torque in Equation (10) involves infinitesimal forces $\boldsymbol{\nu}(x, y)$ but not infinitesimal torques (under bounded forces, torques vanish when application points draw infinitely closer). In other words, our model of surface contacts is a continuum of point contacts.

Accordingly, under Coulomb friction, the inequality constraints for $\boldsymbol{\nu}(x, y)$ are:

- **Unilaterality:** $p(x, y) > 0,$ (11)
- **Non-slippage:** $\|\boldsymbol{\sigma}(x, y)\| \leq \mu\, p(x, y).$ (12)

In the present literature, surface contact is often modeled using sets of contact points. In the light of a continuous model, the proposition below gives a theoretical justification for this practice.

Proposition 1: Assume that the contact surface $\mathcal{S}$ is a convex polygon with vertices $C_1, \ldots, C_N$. If there exists a field $(x, y) \mapsto \boldsymbol{\nu}(x, y)$ satisfying complementary inequalities (11)-(12), then there exists contact forces applied at $C_1, \ldots, C_N$, summing up to the same contact wrench, and satisfying complementary inequalities (6)-(7).

Proof: consider pressure and stress fields summing up to $\boldsymbol{w}$. By convexity, one can find barycentric coordinates $\alpha_1(x, y), \ldots, \alpha_k(x, y)$, *i.e.*, positive functions such that $\sum_i \alpha_i(x, y) = 1$ and each point $C_{xy} \in \mathcal{S}$ can be written $C_{xy} = \sum_i \alpha_i(x, y)C_i$. Then, define for each vertex C_i a force

$$\boldsymbol{f}_i := \int_{\mathcal{S}} \alpha_i(x, y)\boldsymbol{\nu}(x, y)\mathrm{d}x\mathrm{d}y,$$

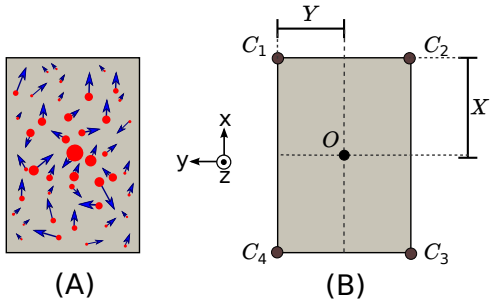

Fig. 2. Contact in the surface plane. (A) Illustration of the stress field (blue arrows) and pressure field (red discs representing magnitude). (B) Notations used in Section IV.

By positivity of the α_i's, it is straightforward to check that all $f_i^n > 0$ and $\|\boldsymbol{f}_i^t\| \leq \mu f_i^n$. In addition, this expression of $\boldsymbol{f}_i$ ensures that the resulting wrenches are equal, *i.e.*, (2) = (9) and (3) = (10). □

If Dirac fields are authorized, then one can show that the converse implication of Proposition 1 is true. If not, whether this converse implication is true remains an open question. The bottom line of this argument is that the forces at the vertices of the convex hull completely render the dynamics of the surface contact. The wrench cone that we derive in the next section will share the same property.

IV. Wrench Cone for Rectangular Surfaces

While the wrench cone could be computed *numerically* for arbitrary contact surfaces by using the face-span manipulations presented in [14], [10][2], the *analytical* formula that we derive below gives insights into the nature of that cone while grounding for more efficient downstream calculations.

Consider a rectangular area $(C_1C_2C_3C_4)$ as depicted in Figure 2 (B). We calculate the contact wrench $\boldsymbol{w}$ at the center O in the link frame. Let us denote by (f_i^x, f_i^y, f_i^z) the three components of the contact force $\boldsymbol{f}_i$ at point C^i, expressed in the link frame. Under the common linear approximation of friction cones, Coulomb inequalities become

$$|f_i^x|, |f_i^y| \leq \mu f_i^z \tag{13}$$

$$f_i^z > 0 \tag{14}$$

The following proposition gives the analytical formulae for the wrench cone.

Proposition 2 (Contact Wrench Cone): There exists a solution $(\boldsymbol{f}_1, \ldots, \boldsymbol{f}_4)$ satisfying inequalities (13)-(14) if and only if there exists a wrench $\boldsymbol{w} = (f^x, f^y, f^z, \tau^x, \tau^y, \tau^z)$ such that:

$$|f^x| \leq \mu f^z \tag{15}$$

$$|f^y| \leq \mu f^z \tag{16}$$

$$f^z > 0 \tag{17}$$

$$|\tau^x| \leq Y f^z \tag{18}$$

$$|\tau^y| \leq X f^z \tag{19}$$

$$\tau^z_{\min} \leq \tau^z \leq \tau^z_{\max} \tag{20}$$

[2]also known as the *double description method*

where

$$\tau^z_{\text{min}} \stackrel{\text{def}}{=} -\mu(X+Y)f^z + |Yf^x - \mu\tau^x| + |Xf^y - \mu\tau^y|,$$
$$\tau^z_{\text{max}} \stackrel{\text{def}}{=} +\mu(X+Y)f^z - |Yf^x + \mu\tau^x| - |Xf^y + \mu\tau^y|.$$

Provided that the kinematic contact equation is satisfied, this condition is necessary and sufficient for weak contact stability.

The proof of this proposition is given in Appendix B. The validity of the formula was also tested empirically with a script available at [15].

Let us now detail each line of the Contact Wrench Cone (CWC). The first two inequalities (15)-(16) correspond to the usual Coulomb friction. Inequalities (17), (18) and (19) are equivalent to having the CoP lie inside of the contact area. The last inequality (20) provides a bound on the admissible yaw torque that was implicitely encoded in the contact-force model.

Observe how this relation is more complex than "no rotation occurs while τ^z is small enough", as it is coupled with all other components of the contact wrench. The yaw torque is bounded by τ^z_{min} and τ^z_{max}, both of which may be either positive or negative (for instance, both become negative when the CoP nears the corner $\tau^x = Yf^z$, $\tau^y = Xf^z$ of the support polygon). Notably, the "safest" value for τ^z is not zero but:

$$\begin{aligned}\tau^z_{\text{safe}} &\stackrel{\text{def}}{=} (\tau^z_{\text{min}} + \tau^z_{\text{max}})/2 \\ &= \text{sgn}(-f^x\tau^x)\min(Y|f^x|, \mu|\tau^x|) \\ &+ \text{sgn}(-f^y\tau^y)\min(X|f^y|, \mu|\tau^y|),\end{aligned}$$

with sgn the sign function. From Equation (20), τ^z may deviate from τ^z_{safe} by at most

$$\mu(X+Y)f^z - \max(Y|f^x|, \mu|\tau^x|) - \max(X|f^y|, \mu|\tau^y|).$$

We see from this rewriting that higher tangential forces or roll-pitch torques reduce the range of admissible yaw torques. In particular, when these other constraints are saturated (*e.g.*, when the CoP reaches a corner of the support polygon), τ^z_{safe} is the *only solution* that prevents the contact from breaking. Therefore, $\tau^z = \tau^z_{\text{safe}}$ appears as a sensible control law to prevent undesired yaw rotations.

V. Experiment

We test the CWC in the dynamics simulator OpenHRP with a model of the HRP4 robot. Note that OpenHRP has its own contact model where forces are distributed along the edges (not corners) of the contact surface.

We enforce the CWC within the Time-Optimal Path Parameterization framework (TOPP), a well-known projection of system dynamics along a pre-defined path that has been used for motion planning of humanoid robots [7], [16], [9]. We considered the case of a single contact at the left foot and designed a motion that would challenge all six contact DOFs. In single contact, the contact wrench is fully determined by the unactuated rows of the equation of motion, *i.e.*,

$$\boldsymbol{w} = (\mathbf{P}\mathbf{J}_{\text{wr}})^{-1}\mathbf{P}\left[\mathbf{M}(\boldsymbol{q})\ddot{\boldsymbol{q}} + \boldsymbol{h}(\boldsymbol{q}, \dot{\boldsymbol{q}})\right]$$

where $\mathbf{P} = \mathbf{I} - \mathbf{S}$ is the $6 \times n$ projector on the free-flying coordinates. The matrix $\mathbf{P}\mathbf{J}_{\text{wr}}$ is non-singular thanks to the use of the contact wrench.

For this experiment, we designed by hand a set of eleven key postures. The geometric path was obtained by interpolating Bezier curves between these postures and using inverse kinematics to fix the position and orientation of the support foot on the ground. To time this path into a trajectory, we used the open-source TOPP solver [17]. The solver takes as input the path and a vector representation of the system dynamics along it, which is easy to compute once one knows the projectors mentioned above (see [9] for details). As is common with numerical TOPP solvers, we added safety margins in the CWC computations input to TOPP: the foot dimensions X and Y were scaled by 70% (versus 100% in OpenHRP) and the friction coefficient set to $\mu = 0.4$ (versus $\mu = 0.8$ in OpenHRP).

Figure 3 shows a timelapse of the final retimed motion. A video is also available online at [15]. Because time optimality yields bang-bang control laws, the retimed motion always saturates at least one of the contact constraints. Therefore, trying to execute it faster should result in the end-effector breaking surface contact, *e.g.*, tipping on the edge of the foot. We observed this phenomenon in the experiment, as depicted in Figure 4. Note that, as we used HRP4's stabilizer while executing the motion, it was still possible in practice to accelerate the motion by about 5% (*i.e.*, reducing the total duration by 5% with uniform time scaling) whithout noticing any change in contact stability.

VI. Conclusion

In this paper, we calculated the closed-form expression of the Contact Wrench Cone for rectangular contact surfaces. This formula has several implications. First, it is very simple, making computations easier than other models based on contact forces. Second, it describes the phenomenon of *yaw friction* by a double inequality that is, to the best of our knowledge, novel. From these bounds, we derived a simple control law to avoid undesired foot rotations, a recurring problem for bipeds in single contact. We also assessed the validity of the CWC condition in dynamics simulations.

The mathematical derivation of the wrench cone formula (Appendix B) can be carried out for parametric shapes other than rectangles. We are surveying this application as part of future work, as well as the combination of local wrench cones into the gravito-inertial wrench [2].

Acknowledgments

This work was partially supported by Tier 1 grant n° RG109/14 awarded by Singapore MOE to the second author.

References

[1] M. Vukobratović and B. Borovac, "Zero-moment pointthirty five years of its life," *International Journal of Humanoid Robotics*, vol. 1, no. 01, pp. 157–173, 2004.

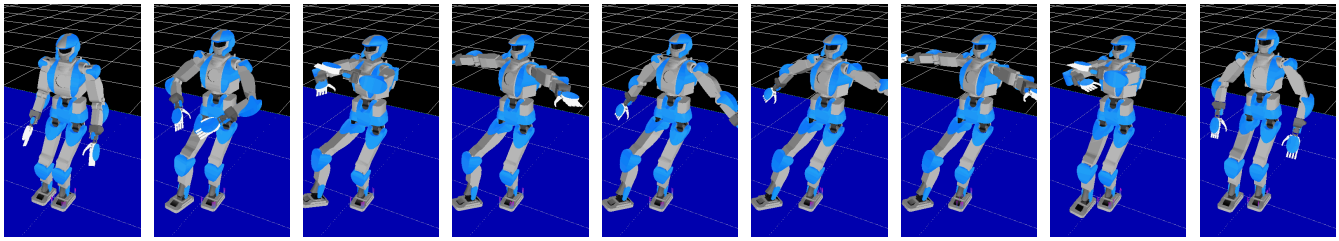

Fig. 3. Snapshots of the retimed motion. Total duration is 7.3 s. Time stamps are shown below each frame. The motion stresses all components of the wrench cone. The first segment stresses the pitch by moving the CoP forward. The second stresses the rool through arm motions. Meanwhile, the yaw component is stressed by chest-pitch motions. Finally, the waist performs an elliptic motion (back and forth, up and down) throughout the whole motion, thus stressing the translation of the contact foot.

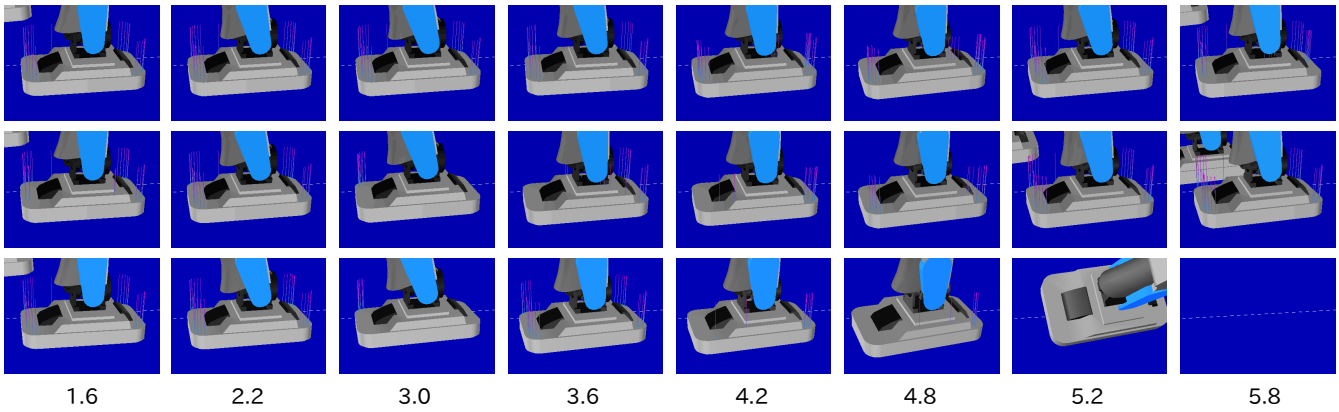

Fig. 4. Zoom on the contact forces computed by OpenHRP at the left foot. Each thin purple segment corresponds to one force. Time stamps are shown below each column. **First row:** retimed motion with CWC enforced. **Second row:** 10% acceleration of the motion, CWC is not enforced. Around 4.2 s, the contact surface degenerates to a line contact on the left edge of the foot. **Third row:** 15% acceleration of the motion, CWC is not enforced. The contact surface degenerates to a line before contact is lost and the humanoid falls.

[2] H. Hirukawa, S. Hattori, K. Harada, S. Kajita, K. Kaneko, F. Kanehiro, K. Fujiwara, and M. Morisawa, "A universal stability criterion of the foot contact of legged robots-adios zmp," in *Robotics and Automation, 2006. ICRA 2006. Proceedings 2006 IEEE International Conference on*. IEEE, 2006, pp. 1976–1983.

[3] B. Ugurlu, J. A. Saglia, N. G. Tsagarakis, and D. G. Caldwell, "Yaw moment compensation for bipedal robots via intrinsic angular momentum constraint," *International Journal of Humanoid Robotics*, vol. 9, no. 04, 2012.

[4] R. Cisneros, K. Yokoi, and E. Yoshida, "Yaw moment compensation by using full body motion," in *Mechatronics and Automation (ICMA), 2014 IEEE International Conference on*. IEEE, 2014, pp. 119–125.

[5] C. Ott, M. A. Roa, and G. Hirzinger, "Posture and balance control for biped robots based on contact force optimization," in *Humanoid Robots (Humanoids), 2011 11th IEEE-RAS International Conference on*. IEEE, 2011, pp. 26–33.

[6] L. Saab, O. E. Ramos, F. Keith, N. Mansard, P. Soueres, and J. Fourquet, "Dynamic whole-body motion generation under rigid contacts and other unilateral constraints," *Robotics, IEEE Transactions on*, vol. 29, no. 2, pp. 346–362, 2013.

[7] K. Hauser, "Fast interpolation and time-optimization with contact," *The International Journal of Robotics Research*, vol. 33, no. 9, pp. 1231–1250, 2014.

[8] L. Righetti, J. Buchli, M. Mistry, M. Kalakrishnan, and S. Schaal, "Optimal distribution of contact forces with inverse-dynamics control," *The International Journal of Robotics Research*, vol. 32, no. 3, pp. 280–298, 2013.

[9] S. Caron, Y. Nakamura, and Q.-C. Pham, "Kinodynamic motion retiming for humanoid robots," in *Proceedings of the 32nd Annual Conference of the Robotics Society of Japan*, 2014.

[10] D. J. Balkcom and J. C. Trinkle, "Computing wrench cones for planar rigid body contact tasks," *The International Journal of Robotics Research*, vol. 21, no. 12, pp. 1053–1066, 2002.

[11] H. Hirukawa, S. Hattori, S. Kajita, K. Harada, K. Kaneko, F. Kanehiro, M. Morisawa, and S. Nakaoka, "A pattern generator of humanoid robots walking on a rough terrain," in *Robotics and Automation, 2007 IEEE International Conference on*. IEEE, 2007, pp. 2181–2187.

[12] Y. Zheng, M. C. Lin, D. Manocha, A. H. Adiwahono, and C.-M. Chew, "A walking pattern generator for biped robots on uneven terrains," in *Intelligent Robots and Systems (IROS), 2010 IEEE/RSJ International Conference on*. IEEE, 2010, pp. 4483–4488.

[13] J.-S. Pang and J. Trinkle, "Stability characterizations of rigid body contact problems with coulomb friction," *ZAMM-Journal of Applied Mathematics and Mechanics/Zeitschrift für Angewandte Mathematik und Mechanik*, vol. 80, no. 10, pp. 643–663, 2000.

[14] S. Hirai, "Analysis and planning of manipulation using the theory of polyhedral convex cones," Ph.D. dissertation, Kyoto University, 1991.

[15] https://scaron.info/research/icra-2015.html, [Online].

[16] Q.-C. Pham, S. Caron, and Y. Nakamura, "Kinodynamic planning in the configuration space via admissible velocity propagation," in *Robotics: Science and Systems*, 2013.

[17] Q.-C. Pham, "A general, fast, and robust implementation of the time-optimal path parameterization algorithm," *IEEE Transactions on Robotics*, vol. 6, pp. 1533–1540, 2014.

APPENDIX

A. Proof of Equation 4

The rotation Jacobian satisfies $\boldsymbol{\omega} = \mathbf{J}_{\text{rot}}\dot{\boldsymbol{q}}$, where $\boldsymbol{\omega}$ is the rotation velocity of the link. As a consequence of this, for any point C on the link and any vector $\boldsymbol{u}$, one has

$$\left(\frac{\partial \overrightarrow{OC}}{\partial \boldsymbol{q}}\right)^{\top} \boldsymbol{u} = \mathbf{J}_{\text{rot}}^{\top} \left(\overrightarrow{OC} \times \boldsymbol{u}\right). \tag{21}$$

Next, the position of any point C_i of the link in the absolute frame is related to that of its origin O by $C_i = O + \overrightarrow{OC_i}$.

The corresponding translation Jacobian is $\mathbf{J}(C_i) = \frac{\partial C_i}{\partial \boldsymbol{q}} = \mathbf{J}(O) + \frac{\partial \overrightarrow{OC_i}}{\partial \boldsymbol{q}}$. Thus,

$$\textstyle\sum_i \mathbf{J}(C_i)^\top \boldsymbol{f}_i = \mathbf{J}(O)^\top \sum_i \boldsymbol{f}_i + \sum_i \left(\frac{\partial \overrightarrow{OC_i}}{\partial \boldsymbol{q}}\right)^\top \boldsymbol{f}_i.$$

The first term of the expression equals the translation component of $\mathbf{J}_{\text{wr}}^\top \boldsymbol{w}$. By applying (21), we see that the second term equals $\mathbf{J}_{\text{rot}}^\top(\overrightarrow{OC_i} \times \boldsymbol{f}_i)$. Factoring $\mathbf{J}_{\text{rot}}^\top$ out of the summation yields the rotation component of $\mathbf{J}_{\text{wr}}^\top \boldsymbol{w}$. □

B. Calculation of the Wrench Cone

The wrench is defined by (2)-(3) as:

$$\begin{array}{rcl} f^x &=& f_1^x + f_2^x + f_3^x + f_4^x \\ f^y &=& f_1^y + f_2^y + f_3^y + f_4^y \\ f^z &=& f_1^z + f_2^z + f_3^z + f_4^z \\ \tau^x &=& Y(f_1^z - f_2^z - f_3^z + f_4^z) \\ \tau^y &=& -X(f_1^z + f_2^z - f_3^z - f_4^z) \\ \tau^z &=& X(f_1^y + f_2^y - f_3^y - f_4^y) - Y(f_1^x - f_2^x - f_3^x + f_4^x). \end{array}$$

By unilaterality (14) we have $f^z > 0$, so we can define:

$$\begin{array}{rclrcl} K_1 &:=& f^x/\mu f^z & C_1 &:=& \tau^x/Y f^z \\ K_2 &:=& f^y/\mu f^z & C_2 &:=& \tau^y/X f^z \\ K_3 &:=& \tau^z/\mu(X+Y) f^z & D_i &:=& f_i^z/\textstyle\sum_i f_i^z \\ p_x &:=& X/(X+Y) & p_y &:=& Y/(X+Y) \\ \alpha_i^x &:=& f_i^x/\mu f_i^z & \alpha_i^y &:=& f_i^y/\mu f_i^z \end{array}$$

and normalize the system by dividing each row accordingly. From the non-slippage constraint (13), we have α_i^x, α_i^y and $D_i \in [-1,1]$. Then, introduce the new variables:

$$\begin{array}{rclrcl} \gamma_x &=& \alpha_1^x D_1 + \alpha_4^x D_4 & \gamma'_x &=& \alpha_2^x D_2 + \alpha_3^x D_3 \\ \gamma_y &=& \alpha_1^y D_1 + \alpha_2^y D_2 & \gamma'_y &=& \alpha_3^y D_3 + \alpha_4^y D_4 \end{array}$$

We can reduce the complete system in two ways. First, using the fact that the relation $\mathbf{M}$ from $\boldsymbol{\alpha}$ to $\boldsymbol{\gamma}$ is a linear surjection from $[-1,1]^8$ to $\mathbf{M}[-1,1]^8 = \{|\gamma_i^{x|y}| \leq D_j + D_k\}$ (the computation of antecedents being straightforward). Since there is no other constraint on the α_i's than their domain and relation to γ_i's, one can obtain an equivalent system by replacing $\boldsymbol{\alpha} \in [-1,1]^8$ by $\boldsymbol{\gamma} \in \mathbf{M}[-1,1]^8$. Then, the three equations in D_i's are:

$$\begin{array}{rcl} 1 &=& D_1 + D_2 + D_3 + D_4, \\ C_1 &=& D_1 - D_2 - D_3 + D_4, \\ C_2 &=& -D_1 - D_2 + D_3 + D_4, \end{array}$$

By linear combination, we can use them to rewrite $\mathbf{M}[-1,1]^8$ as: $2|\gamma_x| \leq 1 + C_1$, $2|\gamma'_x| \leq 1 - C_1$, $2|\gamma_y| \leq 1 - C_2$, $2|\gamma'_y| \leq 1 + C_2$. Finally, using the same equations, one can express all D_i's as functions of, *e.g.*, D_4. The inequalities $\mathbf{D} \in [0,1]^4$ become:

$$\begin{array}{ccccc} -1 + C_1 & \leq & 2D_4 & \leq & 1 + C_1 \\ C_1 + C_2 & \leq & 2D_4 & \leq & 2 + C_1 + C_2 \\ -1 + C_2 & \leq & 2D_4 & \leq & 1 + C_2 \\ 0 & \leq & 2D_4 & \leq & 2 \end{array}$$

This system has solutions if and only if all lower bounds are smaller than all upper bounds. Matching all pairs of lower and upper bounds one by one (we will show an example of this technique below in a more complex situation), one can check that all these inequalities boil down to $C_1 \in [-1,1]$ and $C_2 \in [-1,1]$. The complete system is now:

$$\begin{array}{rclrcl} K_1 &=& \gamma_x + \gamma'_x & K_2 &=& \gamma_y + \gamma'_y \\ K_3 &=& p_x(\gamma_y - \gamma'_y) - p_y(\gamma_x - \gamma'_x) & & & \\ 2|\gamma_x| &\leq& 1 + C_1 & 2|\gamma'_x| &\leq& 1 - C_1 \\ 2|\gamma_y| &\leq& 1 - C_2 & 2|\gamma'_y| &\leq& 1 + C_2 \end{array}$$

And $(C_1, C_2) \in [-1,1]^2$. One can use the first three equations to eliminate the redundant variables γ'_x, γ_y and γ'_y, expressing them as functions of γ_x in the inequality constraints. After simplification, the resulting system is:

$$\begin{array}{rcll} 2p_y\gamma_x &\leq& p_y(1 + C_1) & (22) \\ 2p_y\gamma_x &\leq& p_y(1 - C_1) + 2p_y K_1 & (23) \\ 2p_y\gamma_x &\leq& p_x(1 - C_2) - K_3 + p_y K_1 - p_x K_2 & (24) \\ 2p_y\gamma_x &\leq& p_x(1 + C_2) - K_3 + p_y K_1 + p_x K_2 & (25) \\ 2p_y\gamma_x &\geq& -p_y(1 + C_1) & (26) \\ 2p_y\gamma_x &\geq& -p_y(1 - C_1) + 2p_y K_1 & (27) \\ 2p_y\gamma_x &\geq& -p_x(1 - C_2) - K_3 + p_y K_1 - p_x K_2 & (28) \\ 2p_y\gamma_x &\geq& -p_x(1 + C_2) - K_3 + p_y K_1 + p_x K_2 & (29) \end{array}$$

And $(C_1, C_2) \in [-1,1]^2$. There exist a solution γ_x if and only if all of its lower bounds are smaller than all of its upper bounds. Let us match all pairs of lower bounds (26)-(29) and upper bounds (22)-(25). One can check that:

- (26) ≤ (22) ⇔ $C_1 \geq -1$
- (26) ≤ (23) ⇔ $K_1 \geq -1$
- (26) ≤ (24) ⇔ $K_3 - p_y K_1 + p_x K_2 - p_y C_1 + p_x C_2 \leq 1$
- (26) ≤ (25) ⇔ $K_3 - p_y K_1 - p_x K_2 - p_y C_1 - p_x C_2 \leq 1$
- (27) ≤ (22) ⇔ $K_1 \leq 1$
- (27) ≤ (23) ⇔ $C_1 \leq 1$
- (27) ≤ (24) ⇔ $K_3 + p_y K_1 + p_x K_2 + p_y C_1 + p_x C_2 \leq 1$
- (27) ≤ (25) ⇔ $K_3 + p_y K_1 - p_x K_2 + p_y C_1 - p_x C_2 \leq 1$
- (28) ≤ (22) ⇔ $-K_3 + p_y K_1 - p_x K_2 - p_y C_1 + p_x C_2 \leq 1$
- (28) ≤ (23) ⇔ $-K_3 - p_y K_1 - p_x K_2 + p_y C_1 + p_x C_2 \leq 1$
- (28) ≤ (24) ⇔ $C_2 \leq 1$
- (28) ≤ (25) ⇔ $K_2 \geq -1$
- (29) ≤ (22) ⇔ $-K_3 + p_y K_1 + p_x K_2 - p_y C_1 - p_x C_2 \leq 1$
- (29) ≤ (23) ⇔ $-K_3 - p_y K_1 + p_x K_2 + p_y C_1 - p_x C_2 \leq 1$
- (29) ≤ (24) ⇔ $K_2 \leq 1$
- (29) ≤ (25) ⇔ $C_2 \geq -1$

Consequently, the complete system becomes:

$$\begin{array}{rcl} K_3 &\leq& 1 - p_y K_1 - p_x K_2 - p_y C_1 - p_x C_2 \\ K_3 &\leq& 1 - p_y K_1 + p_x K_2 - p_y C_1 + p_x C_2 \\ K_3 &\leq& 1 + p_y K_1 - p_x K_2 + p_y C_1 - p_x C_2 \\ K_3 &\leq& 1 + p_y K_1 + p_x K_2 + p_y C_1 + p_x C_2 \\ K_3 &\geq& -1 + p_y K_1 + p_x K_2 - p_y C_1 - p_x C_2 \\ K_3 &\geq& -1 + p_y K_1 - p_x K_2 - p_y C_1 + p_x C_2 \\ K_3 &\geq& -1 - p_y K_1 + p_x K_2 + p_y C_1 - p_x C_2 \\ K_3 &\geq& -1 - p_y K_1 - p_x K_2 + p_y C_1 + p_x C_2 \end{array}$$

And $(K_1, K_2, C_1, C_2) \in [-1,1]^4$. In a more concise form, these last eight inequalities can be written

$$\begin{array}{rcl} K_3 &\geq& -1 + p_y|K_1 - C_1| + p_x|K_2 - C_2|, \\ K_3 &\leq& +1 - p_y|K_1 + C_1| - p_x|K_2 + C_2|. \end{array}$$

We conclude by de-normalizing all inequalities. □